Novel pathways in cholesterol metabolism to combat cardiometabolic diseases

Zhou, E.

2

Beneficial effects of brown fat activation on top of PCSK9 inhibition with alirocumab on dyslipidemia and atherosclerosis development in APOE*3-Leiden.CETP mice

Enchen Zhou, Zhuang Li, Hiroyuki Nakashima, Ahlam Choukoud, Sander Kooijman, Jimmy F.P. Berbée, Patrick C.N. Rensen, Yanan Wang

Pharmacol Res 2021; In press

Abstract

Background

Proprotein convertase subtilisin/kexin type 9 (PCSK9) inhibition, by increasing hepatic LDL receptor (LDLR) levels, has emerged as a strategy to reduce atherosclerosis by lowering circulating (V)LDL-cholesterol. We hypothesized that the therapeutic effectiveness of PCSK9 inhibition can be increased by accelerating the generation of VLDL remnants, which typically have a high affinity for the LDLR. Therefore, we aimed to investigate whether accelerating lipolytic processing of VLDL by brown fat activation can further lower (V)LDL and reduce atherosclerosis on top of PCSK9 inhibition.

Methods and results

*APOE*3-Leiden.CETP* mice were fed a Western-type diet and treated with or without the brown fat-activating β3-adrenergic receptor (AR) agonist CL316,243 in presence or absence of the anti-PCSK9 antibody alirocumab during 3 and 12 weeks to evaluate VLDL clearance and atherosclerosis development, respectively. Combined β3-AR agonism and alirocumab further decreased (V)LDL-cholesterol compared to alirocumab alone, as explained by an accelerated plasma clearance of VLDL-cholesteryl esters that were mainly taken up by the liver. In addition, the combination promoted the transfer of VLDL-phospholipids to HDL to a higher extent than alirocumab alone, accompanied by higher plasma HDL-cholesterol levels and increased cholesterol efflux capacity. Collectively, combination treatment non-significantly reduced atherosclerotic lesion area compared to alirocumab alone and largely reduced atherosclerotic lesion area compared to vehicle.

Conclusions

β3-AR agonism enhances the lipoprotein-modulating effects of alirocumab to further improve dyslipidaemia and non-significantly further attenuate atherosclerosis development. Brown fat activation may enhance the therapeutic effects of PCSK9 inhibition in dyslipidemia.

Introduction

Atherosclerotic cardiovascular disease (CVD) is the leading cause of death globally. Dyslipidemia is a well-documented risk factor for atherosclerosis. Despite the effectiveness of cholesterol-lowering therapies, e.g. using statins, 55-75% of cardiovascular events still remain [1-3]. The residual risk is considered to be due to inadequate reduction of low density lipoprotein (LDL)-cholesterol (-C) and triglycerides (TG), in addition to inadequate improvement of high density lipoprotein (HDL) function and inflammation [4]. Therefore, new therapeutic strategies to overcome these limitations are needed.

The hepatic LDL receptor (LDLR) is one of the major proteins involved in plasma cholesterol catabolism. Proprotein convertase subtilisin-like kexin type 9 (PCSK9) is a hepatic protease that attaches to the LDLR to promote its intracellular transport into lysosomes for degradation. Clinical studies showed that individuals with loss of function mutations in PCSK9 have lower levels of LDL-C and lower prevalence of CVD [5, 6], indicating that inhibition of PCSK9 is a promising new strategy for lowering cholesterol levels. In 2015, the U.S. Food and Drug Administration approved the PCSK9 monoclonal antibodies alirocumab and evolocumab for the treatment of hypercholesterolemia. The efficacy of these PCSK9 inhibitors to lower LDL-C reaches up to 55% as monotherapy and up to 61% when added to standard therapy, while also reducing the risk of atherosclerotic CVD [7, 8]. In both heterozygous [9] and homozygous [10] familial hypercholesterolaemic (FH) patients, PCSK9 inhibition reduced LDL-C levels by more than half. However, to maintain a decrease in LDL-C, relatively high doses of PCSK9 antibodies are required by subcutaneous administration, which leads to a high financial burden for patients and insurance companies. Therefore, ongoing research focuses on the development of new PCSK9 inhibitors using siRNA or antisense oligonucleotides, vaccines, and inhibitors of PCSK9 secretion.

Brown fat, which is a metabolically active tissue in mammals including humans [11, 12] and characterized by a large number of mitochondria and small lipid droplets, is also emerging as a promising target to combat cardiometabolic disease. Physiologically, cold exposure activates brown fat by stimulating sympathetic neurons to release noradrenalin that can bind to β-adrenergic receptors such as the β3-adrenergic receptor (β3-AR) on brown adipocytes. Cold exposure also induces the appearance of beige/brite adipocytes within white adipose tissue, a process which is referred to as 'browning' [13, 14]. Brown fat activation via β3-AR agonism facilitates uptake of plasma TG-rich lipoprotein (TRL)-derived fatty acids (FAs) into brown adipocytes for oxidation within mitochondria, and increases hepatic uptake of the generated cholesterol-enriched TRL remnants. By this mechanism, brown fat activation reduces TG and non-HDL-C levels in *APOE*3-Leiden.CETP (E3L.CETP)* mice, a well-established translational hyperlipidemic model with an intact hepatic ApoE-LDLR axis [15-17], which is the predominant pathway for TRL remnant clearance. Since brown fat activation via β3-AR agonism does not influence the hepatic levels of the LDLR [18], the cholesterol-lowering effect of brown fat activation is predominantly attributed to enhanced generation of TRL remnants for subsequent uptake by LDLR.

We hypothesized that, by accelerating lipolytic processing of TRL and rapidly generating TRL remnants that have a high affinity for the LDLR, the levels of which are increased by PCSK9 inhibition, brown fat activation increases the therapeutic effectiveness of PCSK9 inhibition in the treatment of hypercholesterolemia and atherosclerosis. Therefore, we aimed to evaluate the effect of a β3-AR agonist, the PCSK9 inhibitor alirocumab and their combination on lipoprotein metabolism and atherosclerosis development in *E3L.CETP* mice.

Material and methods

Animals and treatments

This study was approved by the Animal Ethical Committee of Leiden University Medical Center, Leiden, The Netherlands (DEC14119.1 and PE.18.034.002). All animal procedures were performed conform to the U.K. Animals (Scientific Procedures) Act, 1986 and associated guidelines, EU Directive 2010/63/EU for animal experiments and the ARRIVE guidelines.

Hemizygous *APOE*3-Leiden* (*E3L*) mice were crossbred with homozygous human cholesteryl ester transfer protein (CETP) transgenic mice to generate heterozygous *E3L.CETP* mice [19]. Mice were group-housed in individually ventilated cages in standard conditions at 22°C room temperature with 40 ± 5% relative humidity and a 12-h light/dark cycle. Water and standard rodent chow were available *ad libitum*, unless indicated. At the age of 10-12 weeks, female mice weighing 20 to 25 g were fed a Western-type diet (WTD; Altromin, Germany) containing 15% cacao butter, 1% corn oil and 0.15% ($wt \cdot wt^{-1}$) cholesterol. Mice were daily handled for 5 min for 1 week before experimentation to minimize stress effects. Mice were selected for treatment randomly and observed without knowledge of the treatments administered. We used female mice because only female *E3L.CETP* mice develop WTD-induced dyslipidemia and atherosclerosis, and therefore have been in use as a well-established disease model [16, 20-22].

In a first experiment, mice were randomized into two groups after a run-in period of 3 weeks on WTD based on body weight, body composition and plasma lipid levels and subsequently received the anti-PCSK9 monoclonal antibody alirocumab (symbol: ab; Sanofi and Regeneron, USA; 1 $mg \cdot kg^{-1}$ body weight $week^{-1}$) or vehicle (0.9% saline) weekly by subcutaneous injections between 14:00 and 16:00 h (week -2). After 2 weeks (week 0), when plasma lipid levels reached a new set point, mice in each treatment group were again randomized into two subgroups based on body weight, body composition and plasma lipid levels and additionally treated with the β3-AR agonist CL316,243 (symbol: β; Tocris Bioscience Bristol, United Kingdom; 20 $\mu g \cdot mouse^{-1}$) or vehicle (0.9% saline) 3 times per week by subcutaneous injections between 14:00 and 16:00 h for additional 12 weeks to evaluate effects on cholesterol metabolism and atherosclerosis development. This resulted in the following four treatment groups: (i) vehicle (ctrl), (ii) anti-PCSK9 antibody (ab), (iii) CL316,243 (β), (iv) anti-PCSK9 antibody + CL316,243 (ab+β) (**Supplemental Figure 1A**). Food intake was determined during the first 3 weeks of treatment, and body weight was measured every three weeks. The order of CL316, 243 or saline treatment was randomized during the whole experiment.

In a second experiment, the effects of these four treatments on plasma clearance and hepatic uptake of TG-rich lipoprotein (TRL)-like particles were investigated. The study set-up was similar to the first experiment, with the exception that mice were treated with CL316,243 or vehicle 5 times per week for 3 weeks. The order of CL316, 243 or saline treatment was randomized during the whole experiment. The concentrations, doses, and frequency of CL316, 243 and anti-PCSK9 antibody were based on previous studies [16, 23] and a dose-finding study, respectively.

In both experiments, before and after treatment body composition (i.e. body fat mass and lean mass) was evaluated by putting conscious mice in a red tube that was scanned within 2 min by EchoMRI (EchoMRI-100; Houston, TX, USA). At the end of both experiments, mice were euthanized by CO_2 suffocation, perfused with ice-cold saline via cardiac perfusion, and various organs were isolated for further analysis.

In both experiments, sample sizes of all groups were equal (n = 11 mice per group). Mice/samples were excluded from statistical analysis (exclusion criteria) owing to technical failure,

including unsuccessful intravenous injection and poor histological quality, which has been clearly described in the figure legends.

Plasma lipid assays and lipoprotein profiles

Blood (75 µL) was collected from the lateral tail vein of 4 h-fasted mice into heparin-coated capillaries that were subsequently placed on ice and centrifuged. Plasma was assayed for TG and total cholesterol (TC) using enzymatic kits from Roche Diagnostics (Mannheim, Germany). To measure HDL-cholesterol (C), ApoB-containing lipoproteins were precipitated from plasma using 20% polyethylene glycol 6,000 in 200 mM glycine buffer (pH 10). HDL-C was measured in the supernatant as described for TC. Plasma non-HDL-cholesterol (non-HDL-C) levels were calculated by subtraction of HDL-C from TC levels. Plasma TG and cholesterol exposure was calculated as the area under the curve of plasma TG/TC/non-HDL-C during the vehicle or CL316,243 treatment period. The distribution of cholesterol over lipoproteins was determined in pooled plasma of each treatment group by fast-performance liquid chromatography using a Superose 6 column (GE Healthcare, Piscataway, NJ, USA).

Plasma PCSK9 assay

In the second experiment, blood (75 µL) was collected from the lateral tail vein of 4 h-fasted mice after 3 weeks of vehicle or CL316,243 treatment. Plasma PCSK9 levels were determined using a commercially available ELISA kit (R&D system, Minneapolis, MN, USA) according to the manufacturer's protocol.

Western blotting

From each group of 11 mice of the second experiment, 6 liver samples were randomly chosen. Pieces of snap-frozen liver tissue (50 mg) were lysed in 400 µL RIPA buffer containing 150 mM NaCl, 1.0% NP-40, 0.5% sodium deoxycholate, 0.1% sodium dodecyl sulphate and phosphatase inhibitor cocktail (Piece Thermo Fisher Scientific, IL, USA). Each sample was homogenized with glass beads at 6.5 $m \cdot sec^{-1}$ with Advanced Bench-Top Bead Beating Lysis System (MP biomedicals, CA, USA) for 20 sec. Samples were then centrifugated at 16,200 g for 15 min at 4°C to remove debris, protein concentration in the supernatant was determined using a bicinchoninic acid protein assay (Piece Thermo Scientific, IL, USA), and samples were diluted with sample buffer (Wes, ProteinSimple, CA, USA) to reach a protein concentration of 0.2 $\mu g \cdot \mu L^{-1}$ for subsequent Western blotting. Western blots for LDLR and GAPDH were performed separately with capillary electrophoresis immunoassay using 12 – 230 kDa capillary cartridges (Wes, ProteinSimple, CA, USA) according to the manufacturer's protocol (https://www.proteinsimple.com/ebooks.html). 3 µL of protein samples (0.2 $\mu g \cdot \mu L^{-1}$), 10 µL goat IgG anti-mouse LDLR (RRID: AB_355203; 4 $\mu g \cdot mL^{-1}$, Catalog: AF2255, R&D system, USA) or 10 µL rabbit IgG anti-mouse GAPDH (RRID: AB_10167668; 4 $\mu g \cdot mL^{-1}$, Catalog sc-25778, Santa Cruz, USA) were loaded in pre-filled plates. 10 µL anti-goat or anti-rabbit secondary antibodies from Detection Module kits (DM-006 and DM-001, ProteinSimple, CA, USA) were used per sample. Plates were then centrifuged at 1,000 g for 5 min at room temperature to spin down liquid to the bottom of the wells. No solutions or reagents were reused in this experiment. LDLR and GAPDH protein levels were quantified separately by Compass for SW 4.0.1 (ProteinSimple, CA, USA) automatically. Data were presented as peak area of LDLR and GAPDH separately (fold of the control mean).

***In vivo* plasma decay and hepatic uptake of TG-rich lipoprotein-like particles**

TG-rich lipoprotein (TRL)-like particles (80 nm), labeled with [^{14}C]cholesteryl oleate ([^{14}C]CO), were prepared as described previously [24]. After 3 weeks of treatment with vehicle or

CL316,243 (second experiment), mice were fasted for 4 h (from 9.00 am to 13.00 pm) and injected (t = 0) via the lateral tail vein with 200 µL of TRL-like particles (1 mg TG per mouse). Blood samples (approx. 25 µL) were taken from the lateral tail vein at 2, 5, 10 and 15 min after injection to determine the plasma decay of [^{14}C]CO. After 15 min, mice were perfused with ice-cold saline, livers and other organs were isolated and weighed, and ^{14}C-activity was quantified. Mice were not included for further analysis when intravenous injection failed.

***In vivo* transfer and clearance of surface phospholipid of TRL-like particles**

TRL-like particles (80 nm) were prepared as described previously [24] and labeled with [^{3}H] dipalmitoylphosphatidylcholine (DPPC; PerkinElmer, USA). After 12 weeks of vehicle or CL316,243 treatment (first experiment), mice were fasted for 4 h and injected (t = 0) via the lateral tail vein with 200 µL of TRL-like particles (1 mg TG per mouse). Blood samples (approx. 25 µL) were taken from the lateral tail vein at 2, 5, 10 and 15 min after injection to determine the plasma decay of [^{3}H]DPPC. To measure the transfer of [^{3}H]DPPC onto HDL, ApoB-containing lipoproteins were precipitated from plasma with 20% polyethylene glycol 6,000 in 200 mM glycine buffer (pH 10), and ^{3}H-activity in supernatant was quantified. Mice were not included for further analysis when intravenous injection failed.

***In vitro* HDL cholesterol efflux capacity assay**

Cholesterol efflux capacity was measured as described previously [25]. The human monocyte cell line THP-1 was obtained from European Collection of Cell Cultures (ECACC; RRID: CVCL_0006), and maintained in RPMI 1640 Glutamax medium containing 10% fetal bovine serum, 100 U·mL^{-1} penicillin and 100 µg·mL^{-1} streptomycin at 37°C in 5% CO_2. THP-1 cells were differentiated into macrophages by the addition of 100 nmol·L^{-1} phorbol 12-myristate-13-acetate (PMA; Sigma Aldrich, USA) within 3 days. Macrophages were then washed 3 times with phosphate buffered saline (PBS) and incubated in RPMI 1640 Glutamax medium containing 2% fetal bovine serum, 100 U·mL^{-1} penicillin and 100 µg·mL^{-1} streptomycin, 50 µg protein·mL^{-1} acetyl-LDL and 1 µCi·mL^{-1} [1α,2α(n)-^{3}H]cholesterol (Perkin Elmer, The Netherlands) for 2 days at 37°C in 5% CO_2 to generate macrophage foam cells. After incubation, cells were washed 3 times with PBS and a cholesterol efflux assay was started by adding 2% ApoB-depleted mouse plasma (first experiment after 12 weeks of treatment) in RPMI 1640 Glutamax medium supplemented with 100 U·mL^{-1} penicillin,100 µg·mL^{-1} streptomycin and 0.5 mg·mL^{-1} BSA. Each assay was carried out in triplicate. Efflux to a standard preparation of HDL (50 µg protein·mL^{-1}) was used to correct for plate-to-plate variation. After 6 hours incubation, medium was collected and centrifuged. ^{3}H-activity was quantified by liquid scintillation counting. Total cellular ^{3}H-activity was measured after dissolving the cells with 0.1 M NaOH. Background values (i.e. efflux in the absence of plasma) were subtracted. Cholesterol efflux capacity was calculated by dividing the ^{3}H-activity in the medium by the sum of ^{3}H-activity in the medium and the cell homogenate.

Atherosclerosis plaque characterization and quantification

After 12 weeks of treatment (first experiment), hearts were collected, fixed in phosphate-buffered 4% formaldehyde, and embedded in paraffin. Four sections of the aortic root area with 50 µm-intervals were used and stained with haematoxylin-phloxine-saffron for histological analysis. Lesions were categorized for lesion severity according to the guidelines of the American Heart Association adapted for mice [26] and classified as mild lesions (types 1 - 3) and severe lesions (types 4 - 5). Monoclonal mouse antibody M0851 (RRID: AB_2223500; 1:800, Catalog M0851, Dako, Heverlee, The Netherlands) against smooth muscle cell (SMC) actin was used to quantify the SMC area. A Envision System-HRP labelled

polymer anti-mouse kit (Catalog K4001, Dako, Heverlee, The Netherlands) was used to detect primary antibody. Macrophage area was determined using rat anti-mouse antibody MAC3 (RRID: AB_393587; Catalog 550292, 31.25 ng·mL^{-1}, BD Pharmingen, San Diego, CA, USA) which was detected by a ImmPRESS goat anti-rat IgG polymer kit (Catalog MP-7444, Vector Laboratories, CA, USA). Sirius Red staining was used to quantify the collagen area. Lesion area and composition were determined with Image J Software (version 1.50i). The lesion stability index was determined as the ratio of stable markers (smooth muscle cell area and collagen area) to unstable marker (macrophage area). Mice were not included for further analysis when histological quality was poor.

Materials

The anti-PCSK9 monoclonal antibody alirocumab was purchased from Sanofi and Regeneron, USA and was diluted into 0.22 mg·mL^{-1} in 0.9% saline before administration. CL316,243 compound was purchased from Tocris Bioscience Bristol, UK were dissolved in 0.9% saline at 0.22 mg·mL^{-1} and store at -20°C. All solutions were prewarmed at room temperature before the injection. Enzymatic kits to measure plasma TG and TC levels were from Roche Diagnostics, Germany. PCSK9 ELISA kit was from R&D system, USA. Anti-mouse LDLR (RRID: AB_355203) and GAPDH (RRID: AB_10167668) were from R&D system and Santa Cruz, USA, respectively. Secondary antibodies and other solutions for Western blotting were from commercial kits, ProteinSimple, USA. Anti-mouse antibody against SMC actin (RRID: AB_2223500) was purchased from Dako, The Netherlands. Anti-mouse antibody against MAC3 (RRID: AB_393587) was purchased from BD Pharmingen, USA. Human monocyte cell line THP-1 (RRID: CVCL_0006) was obtained from European Collection of Cell Cultures.

Data and statistical analysis

Experiments were designed to generate groups of equal size and group size is the number of independent values. All samples were blinded and randomly distributed before each assay. Differences between four groups were determined using one-way analysis of variance (ANOVA) with the *LSD post hoc* test if F achieved statistical significance ($P < 0.05$) and there was no significant variance inhomogeneity. The square root (SQRT) of the lesion area was transformed and univariate regression of analyses was performed to test for significant correlations between atherosclerotic lesion area and plasma TG/TC/non-HDL-C exposure as well cholesterol efflux rate. Multiple regression analysis was performed to predict the contribution of plasma TG/TC/non-HDL-C exposure and cholesterol efflux capacity to the atherosclerotic lesion area. Probability values less than 0.05 were considered statistically significant. All statistical analyses were performed with the GraphPad Prism 8.0.1 for Windows except for univariate and multiple regression analyses which were performed with SPSS 25 for Windows.

Results

β3-AR agonism enhances cholesterol-lowering effects of alirocumab

To evaluate the effects of brown fat activation on top of anti-PCSK9 treatment on cholesterol metabolism and atherosclerosis development, WTD-fed *E3L.CETP* mice fed a WTD pretreated with vehicle (ctrl), or the anti-PCSK9 antibody alirocumab (ab) from week -2, were cotreated with vehicle or the β3-AR agonist CL316,243 (β) for 12 additional weeks (**Supplemental Figure 1A**). β3-AR agonism without or with alirocumab marginally increased food intake

(+9%, β vs. ctrl; +10%, ab+β vs. ctrl; **Supplemental Figure 1B**) and decreased total body weight (-9%, β vs. ctrl; -10%, ab+β vs. ctrl; **Supplemental Figure 1C**), accompanied by decreased body fat mass (**Supplemental Figure 1D**) without effects on body lean mass (**Supplemental Figure 1E**). β3-AR agonism alone, and on top of alirocumab, clearly reduced gonadal white adipose tissue (gWAT) weight (**Supplemental Figure 1F**).

Plasma lipid levels were monitored every 3 weeks during the 12 weeks (co)treatment and lipid exposures were calculated as the area under the curve of lipid levels. While alirocumab did not influence plasma triglyceride (TG) levels and TG exposure, β3-AR agonism alone decreased plasma TG levels (**Figure 1A**) and TG exposure (-45%, β vs. ctrl; **Figure 1D**) as we previously reported [16, 18]. β3-AR agonism on top of alirocumab lowered plasma TG levels (**Figure 1A**) and TG exposure to a similar extent as β3-AR agonism alone did (-51%, ab+β vs. ctrl; **Figure 1D**). As compared to vehicle, both alirocumab and β3-AR agonism alone lowered plasma total cholesterol (TC) levels (**Figure 1B**), resulting in reduced TC exposure (-17% and -12%, vs. ctrl; **Figure 1E**). Notably, β3-AR agonism on top of alirocumab further lowered plasma TC levels (**Figure 1B**) and TC exposure as compared to vehicle (-38%) and each single treatment (-25%, ab+β vs. ab; -30%, ab+β vs. β; **Figure 1E**). Furthermore, both alirocumab and β3-AR agonism alone lowered plasma non-HDL-C levels (**Figure 1C**), which resulted in reduced plasma non-HDL-C exposure (-19% and -16%, vs. ctrl; **Figure 1F**). As compared to alirocumab or β3-AR agonism alone, combination treatment further lowered plasma non-HDL-C levels (**Figure 1C**) and non-HDL-C exposure (-33%, ab+β vs. ab; -35%, ab+β vs. β; **Figure 1F**).

β3-AR agonism on top of alirocumab increases TRL remnant clearance via enhancing uptake by the liver

We next explored how β3-AR agonism enhances the non-HDL-C-lowering effects of anti-PCSK9 treatment. While β3-AR agonism did not influence plasma PCSK9 levels, alirocumab alone and in combination with β3-AR agonism largely increased plasma PCSK9 levels (5-6-fold; **Figure 2A**). In the liver, alirocumab increased LDL receptor (LDLR) protein levels (+24%, ab vs. ctrl; **Figure 2B**) without affecting GAPDH protein levels (**Supplemental Figure 2A**). We next investigated if the increased hepatic LDLR levels can functionally accelerate cholesterol-enriched TRL remnant uptake upon brown fat activation [16]. As compared to vehicle, both β3-AR agonism alone and β3-AR agonism in combination with alirocumab accelerated the clearance of TRL-like remnant particles from circulation (**Figure 2C**). The hepatic uptake of these remnants was increased by alirocumab alone (+21%), β3-AR agonism alone (+23%) and the combination treatment (+36%) as compared to vehicle treatment (**Figure 2D). β3-AR agonism in combination with** alirocumab increased TRL remnant uptake into subscapular brown adipose (sBAT) as compared to control (+42%) and alirocumab alone (+91%). The TRL remnant uptake by various organs/tissues is described in **Supplemental Figure 2B**.

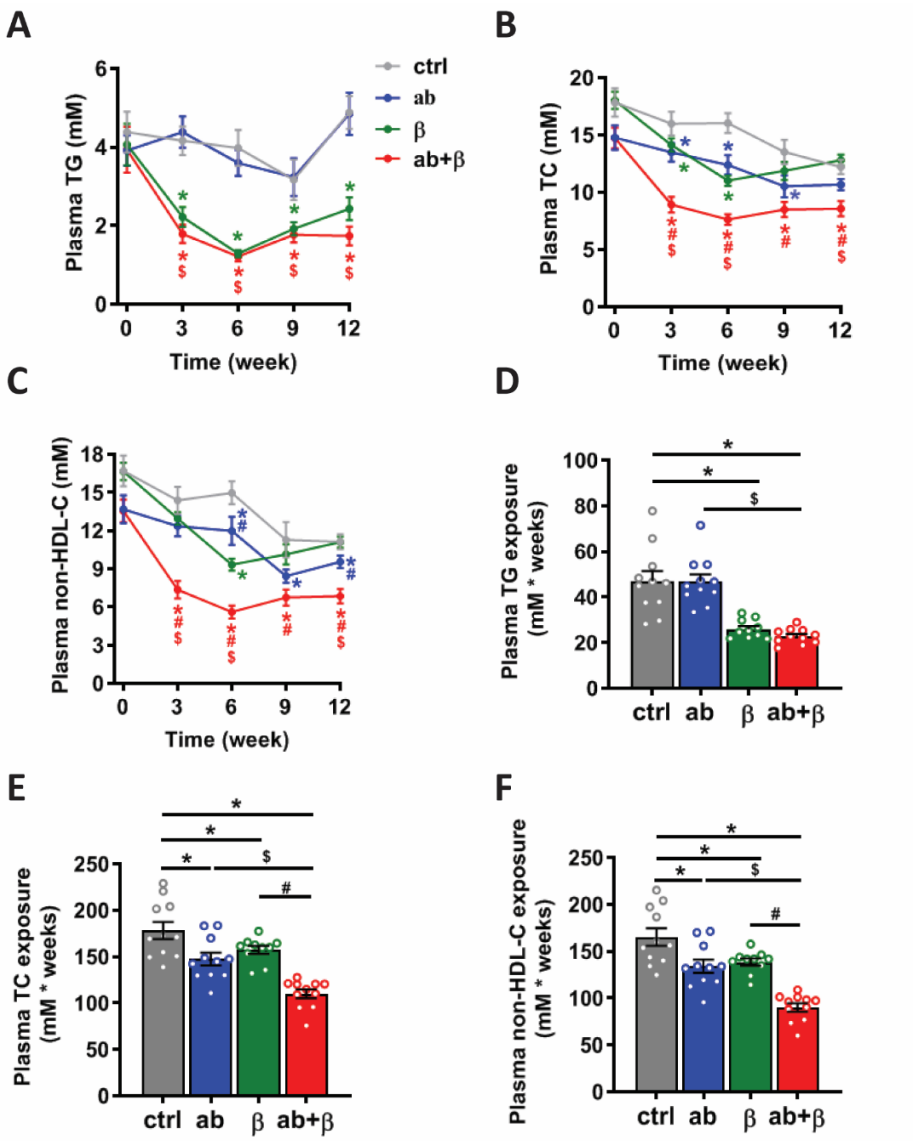

Figure 1. β3-AR agonism on top of anti-PCSK9 treatment further reduces plasma non-HDL cholesterol levels. *E3L.CETP* mice fed a WTD and pretreated with vehicle (ctrl) or the anti-PCSK9 antibody alirocumab (ab) from week -2, were cotreated with vehicle or the β3-AR agonist CL316,243 (β) from week 0 for 12 additional weeks. Blood was collected to determine plasma (**A**) triglycerides (TG), (**B**) total cholesterol (TC), and (**C**) non-HDL-cholesterol (-C) levels at the indicated time points. (**D**) TG exposure, (**E**) TC exposure, and (**F**) non-HDL-C exposure were calculated. n = 11, 11, 10, 11 mice respectively. One mouse was excluded due to loss of the blood sample. Values are means ± SEM. Differences between 4 groups were determined using one-way ANOVA with the *LSD post hoc* test. *P<0.05 vs. vehicle (ctrl); $P<0.05 vs. anti-PCSK9 antibody (ab); #P<0.05 vs. β3-AR agonist (β).

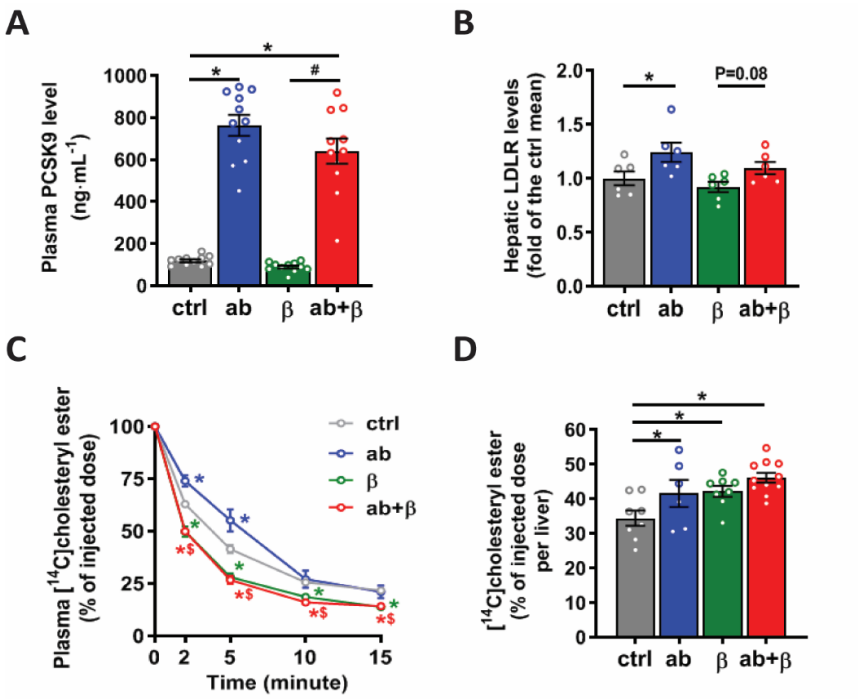

Figure 2. β3-AR agonism on top of anti-PCSK9 treatment increases TRL remnant clearance via enhancing uptake by the liver. *E3L.CETP* mice fed a WTD and pretreated with vehicle (ctrl) or the anti-PCSK9 antibody alirocumab (ab) from week -2, were cotreated with vehicle or the β3-AR agonist CL316,243 (β) from week 0. At week 3, (**A**) plasma PCSK9 (n = 11 in each group) and (**B**) hepatic LDL receptor (LDLR) protein levels (6 mice were randomly selected from each group) were measured. GAPDH protein levels were measured separately as loading control (Supplemental Figure 2A). Mice were injected with [^{14}C]cholesteryl oleate (CO)-labelled TRL-like particles, and (**C**) plasma clearance of [^{14}C]CO, and (**D**) hepatic uptake of [^{14}C]CO after 15 min were measured (n = 8, 6, 8, and 11 mice respectively). Mice were excluded in case of technical failure of intravenous injection. Values are means ± SEM. Differences between 4 groups were determined using one-way ANOVA with the *LSD post hoc* test. *P<0.05 vs. vehicle (ctrl); $^{\$}$P<0.05 vs. anti-PCSK9 antibody (ab); $^{\#}$P<0.05 vs. β3-AR agonist (β).

β3-AR agonism on top of alirocumab accelerates surface phospholipid transfer to HDL, increases HDL levels and HDL cholesterol efflux capacity *in vitro*

The cholesterol distribution over lipoproteins showed that besides decreasing non-HDL-C (fractions 0-15), **β3-AR agonism alone and in combination with** alirocumab increased HDL-C (fractions 15-25) (**Figure 3A**). Indeed, both **β3-AR agonism alone and in combination with** alirocumab increased plasma HDL-C levels and HDL-C exposure compared to vehicle treatment (+45%, β vs. ctrl; +47%, ab+β vs. ctrl), while alirocumab alone had no effect (**Figure 3B-C**). These observations are in line with our previous studies showing that brown fat activation by cold exposure or **β3-AR agonism** increases HDL-C levels [16, 27]. We hypothesized that brown fat activation-mediated lipolytic processing of TRL particles results in the release of phospholipids that are transferred into HDL particles thus increasing HDL

remodeling. To test this hypothesis, we injected mice with [^{3}H]dipalmitoylphosphatidylcholine (DPPC)-labeled TRL-like particles. As compared to vehicle and alirocumab alone, both **β3-AR agonism alone and in combination with** alirocumab accelerated [^{3}H]DPPC clearance from the circulation, related to increased hepatic remnant removal (**Figure 3D**). **β3-AR agonism increased the** [^{3}H]DPPC fraction in HDL as compared to control group (**Figure 3E**). alirocumab slightly increased the [^{3}H]DPPC fraction in HDL, which was further enhanced by **β3-AR agonism treatment** (**Figure 3E**). Next, the cholesterol efflux capacity of HDL was evaluated *in vitro* using cholesterol-laden THP-1 cells incubated with ApoB-depleted plasma from the first animal experiment. We found that the cholesterol efflux capacity of HDL was increased by **β3-AR agonism alone (+19%, β vs. ctrl) and on top of** alirocumab (+23%, ab+β vs. ctrl; +19%, ab+β vs. ab) (**Figure 3F**). Taken together, combined **β3-AR agonism** with alirocumab increased HDL-C levels related to increased phospholipid transfer to HDL, and increased the cholesterol efflux capacity of HDL.

β3-AR agonism on top of alirocumab non-significantly further reduces atherosclerosis development, and largely attenuates atherosclerosis compared to vehicle treatment

Next, we investigated if the further decreased plasma non-HDL-C levels and increased HDL functionality resulting from the combination therapy as compared to single treatments alone are accompanied by attenuation of atherosclerosis progression. The aortic roots of the hearts were isolated and stained to evaluate atherosclerotic lesion area and severity. As compared to vehicle, alirocumab alone, β3-AR agonism alone, and the combination treatment decreased atherosclerotic lesion area throughout the aortic root (**Figure 4A, B**), resulting in lower mean atherosclerotic lesion area (-62%, -32%, -72% respectively; **Figure 4C**). In addition, β3-AR agonism on top of alirocumab further reduced mean atherosclerotic lesion area by 27% as compared to alirocumab alone, although statistical significance was not reached (**Figure 4C**). The non-HDL-C-lowering effects largely explained the protection of atherosclerosis development as the non-HDL-C exposure was strongly associated with the square root (SQRT) of atherosclerotic lesion area (R^2=0.47; P<0.05, **Figure 4D**). A marginal association was detected between plasma TG exposure and SQRT of lesion area (R^2=0.09; P=0.05, **Figure 4E**), while no significant association was found between plasma HDL-C exposure or HDL cholesterol efflux capacity and SQRT of lesion area (**Supplemental Figure 3A, B**). Additionally, alirocumab combined with β3-AR agonism reduced atherosclerotic lesion severity by increasing mild lesions and decreasing severe lesions (**Figure 4F**).

We further characterized atherosclerotic lesion composition by quantifying the relative plaque content of smooth muscle cells, collagen, and macrophages. Relative smooth muscle cell area (**Figure 5A, B**), collagen area (**Figure 5A, C**) and macrophage area (**Figure 5A, D)** were not affected by any of the treatments. In addition, none of the treatments influenced the lesion stability index, as calculated from the ratio of stable markers (i.e. smooth muscle cell and collagen area) versus the unstable marker (i.e. macrophage area). Taken together, while β3-AR agonism non-significantly increased the anti-atherogenic effect of alirocumab, the combination of alirocumab and β3-AR agonism largely reduced atherosclerotic lesion area and lesion severity.

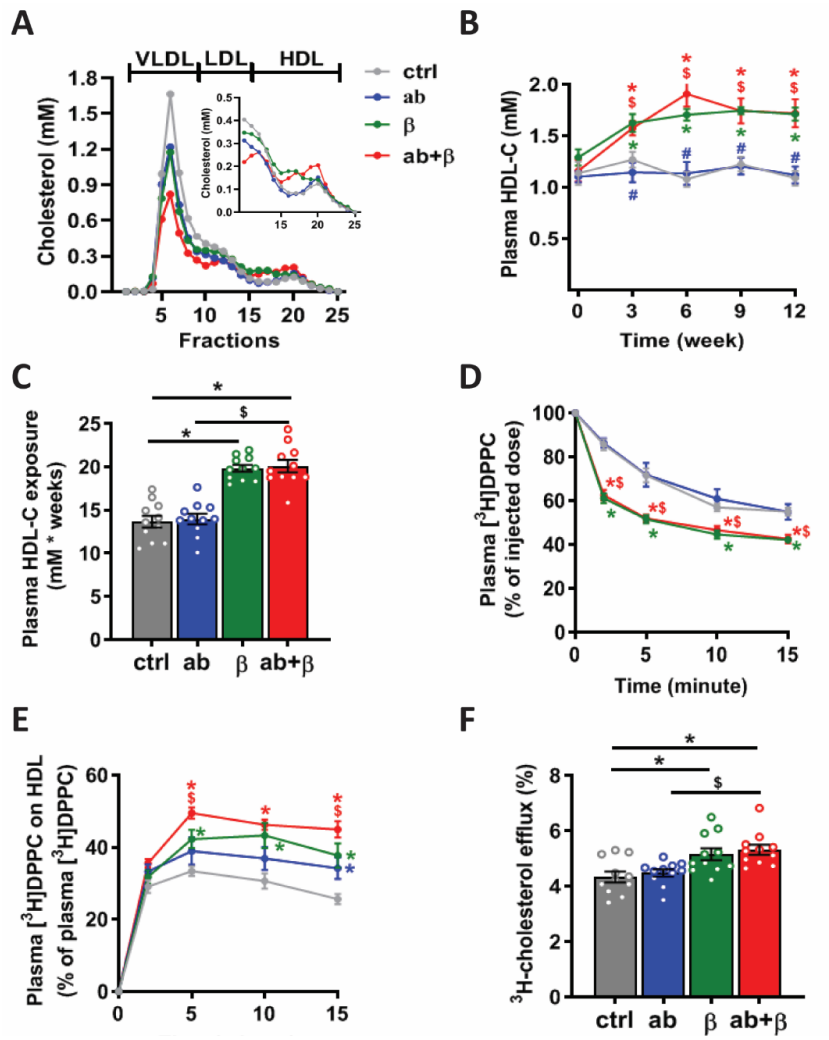

Figure 3. β3-AR agonism on top of anti-PCSK9 treatment accelerates surface phospholipid transfer from TRL-like particles to HDL, increases HDL-C levels, and enhances cholesterol efflux capacity of HDL. *E3L.CETP* mice fed a WTD and pretreated with vehicle (ctrl) or the anti-PCSK9 antibody alirocumab (ab) from week -2, were cotreated with vehicle or the β3-AR agonist CL316,243 (β) from week 0. (**A**) At week 12, blood samples were collected and pooled per group to determine cholesterol distribution over lipoproteins. (**B**) Plasma HDL cholesterol (-C) levels were measured at the indicated time points and (**C**) HDL-C exposure was calculated accordingly (n = 11 mice per group). At the end of week 12, mice were injected with [^{3}H]dipalmitoylphosphatidylcholine (DPPC)-labelled TRL-like particles and (**D**) plasma clearance of [^{3}H]DPPC was determined. HDL was isolated and (**E**) the fraction of [^{3}H]DPPC in HDL was calculated at the indicated time points after particle injection (n = 10, 11, 10 and 10 mice, respectively). Mice were excluded in case of technical failure of injection. (**F**) HDL cholesterol efflux capacity was evaluated using ApoB-depleted plasma (n = 11 mice per group). Values are means ± SEM. Differences between 4 groups were determined using one-way ANOVA with the *LSD post hoc* test. *P<0.05 vs. vehicle (ctrl); $^{\$}$P<0.05 vs. anti-PCSK9 antibody (ab); $^{\#}$P<0.05 vs. β3-AR agonist (β).

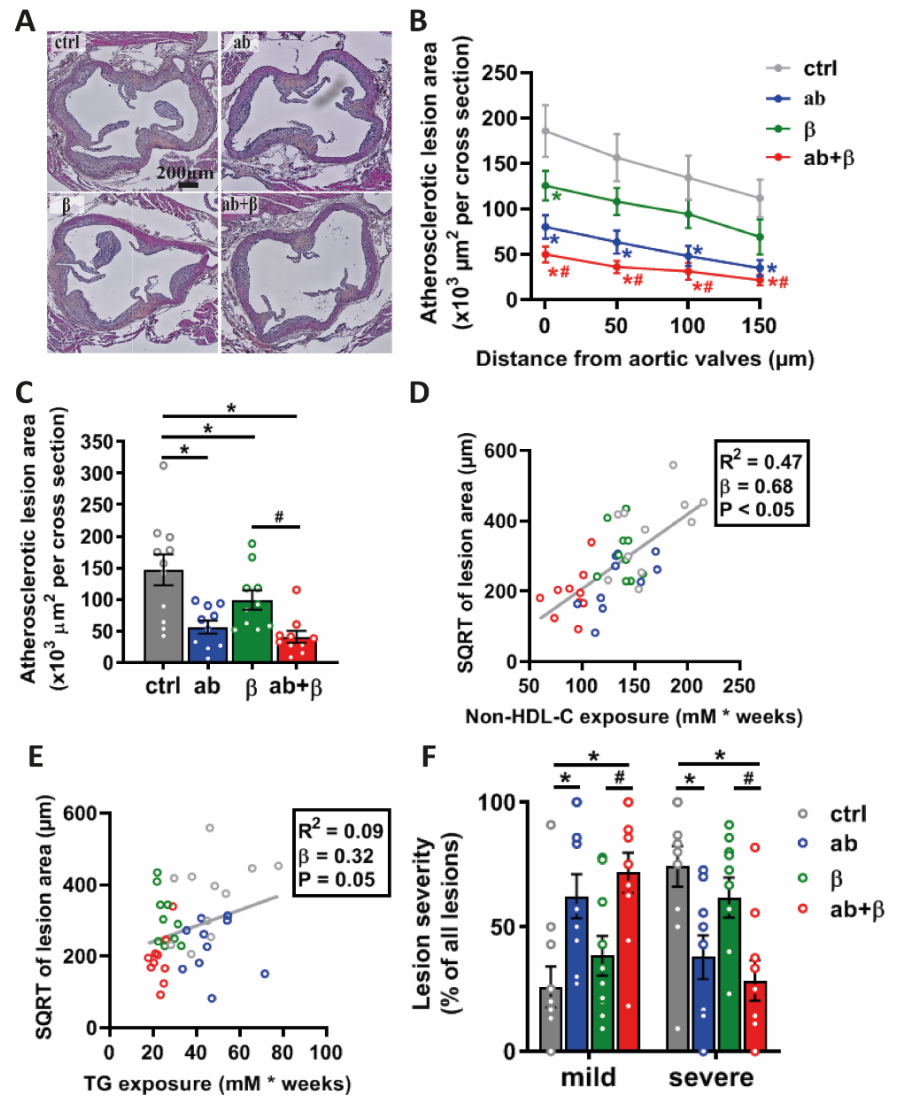

Figure 4. β3-AR agonism on top of anti-PCSK9 treatment reduces atherosclerotic lesion area and lesion severity. *E3L.CETP* mice fed a WTD and pretreated with vehicle (ctrl) or the anti-PCSK9 antibody alirocumab (ab) from week -2, were cotreated with vehicle or the β3-AR agonist CL316,243 (β) from week 0 for 12 additional weeks. (**A**) Cross-sections of the aortic roots were stained with hematoxylin-phloxine-saffron and representative pictures of atherosclerotic lesions of each group are presented. From these pictures, (**B**) plaque lesion area as a function of distance from the appearance of open valves and (**C**) mean atherosclerotic lesion area were calculated. The square root (SQRT) of the mean atherosclerotic lesion area was plotted against the plasma (**D**) non-HDL cholesterol (-C) exposure and (**E**) TG exposure. (**F**) Lesions were categorized according to lesion severity (n = 11, 10, 10 and 10 mice, respectively). Three samples were lost due to technical failure of staining. Values are means ± SEM. Differences between 4 groups were determined using one-way ANOVA with the *LSD post hoc* test. *P<0.05 vs. vehicle (ctrl); #P<0.05 vs. β3-AR agonist (β).

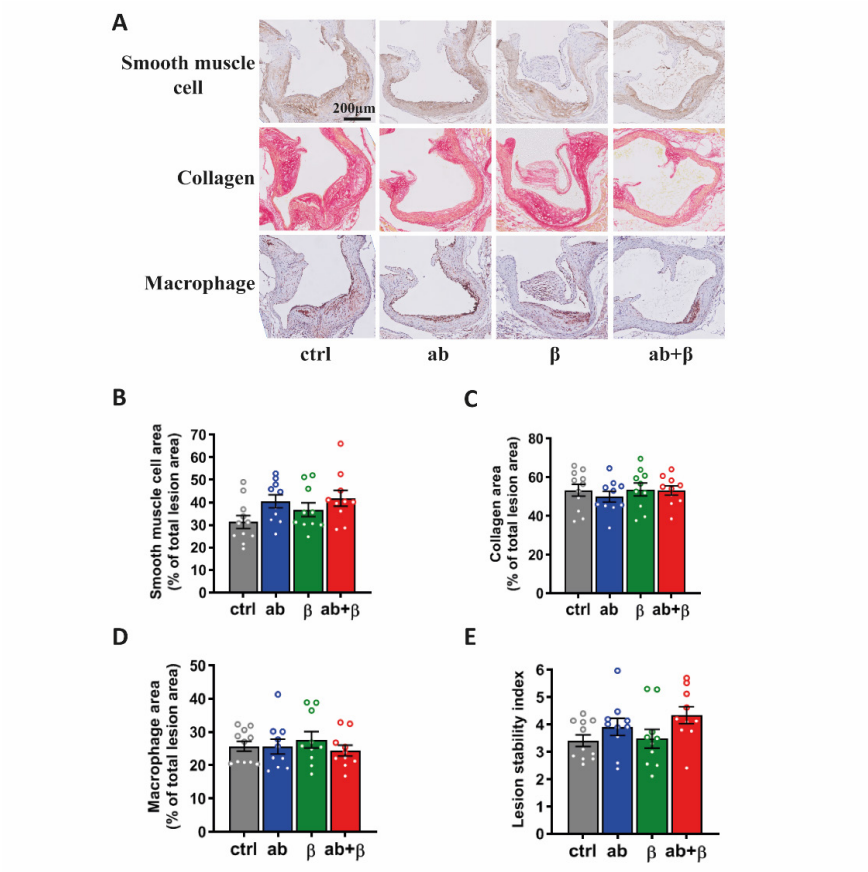

Figure 5. β3-AR agonism on top of anti-PCSK9 treatment does not influence atherosclerotic plaque composition and stability. *E3L.CETP* mice fed a WTD and pretreated with vehicle (ctrl) or the anti-PCSK9 antibody alirocumab (ab) from week -2, were cotreated with vehicle or the β3-AR agonist CL316,243 (β) from week 0 for 12 additional weeks. Cross-sections of aortic root were stained for (**A, B**) smooth muscle cells, (**A, C**) collagen and (**A, D**) macrophages, and their relative areas within the lesions were quantified. (**E**) The plaque stability index was calculated as the ratio of stable markers (i.e. smooth muscle cell area and collagen area) to unstable marker (i.e. macrophage area) (n = 11, 10, 10 and 10 mice, respectively). Three samples were lost due to technical failure of staining. Values are means ± SEM. Differences between 4 groups were determined using one-way ANOVA with the *LSD post hoc* test.

Discussion

Considerable evidence demonstrates that more effective LDL-C lowering further reduces atherosclerotic burden supporting the notion "the lower, the better" for LDL-C levels. While the anti-PCSK9 antibodies alirocumab and evolocumab lower cholesterol levels effectively [7, 28], room remains for additional LDL-C lowering. Here we showed that activating brown fat increases the (V)LDL-C-lowering efficacy of anti-PCSK9 treatment using alirocumab. This effect is probably exerted by a more efficient hepatic uptake of generated cholesterol-

enriched TRL remnants that can subsequently be taken up via the more functional hepatic LDLR pathway, although this effect did not reach significance. Additionally, adding brown fat activation to alirocumab, through surface phospholipid transfer to HDL, increased HDL functionality with respect to its capacity to induce cholesterol efflux. Although brown fat activation non-significantly attenuated atherosclerosis development compared to alirocumab alone, combining brown fat activation with alirocumab largely reduced atherosclerosis development as compared to vehicle.

Previously we showed that brown fat activation enhances TRL remnant formation in mice [29]. In mice without an intact hepatic ApoE/LDLR pathway, such as *Apoe*$^{-/-}$ and *Ldlr*$^{-/-}$ mice, these generated TLR remnants cannot be efficiently taken up by the liver, thus exacerbating hyperlipidemia and atherosclerosis development [30]. In favorable contrast, β3-AR agonism improves hepatic TRL remnant clearance, hypercholesterolemia and atherosclerosis in our *E3L.CETP* mice, as they have an intact ApoE/LDLR pathway [16]. Although **β3-AR agonism** per se does not increase hepatic LDLR levels [16], TRL remnants are rich in ApoE and therefore have a high binding affinity to hepatic LDLR to facilitate TRL remnant removal. Since we hypothesized that an increase in hepatic lipoprotein receptors would accelerate removal of these TRL remnants, we now combined brown fat activation with PCSK9 inhibition to increase hepatic LDLR. Alirocumab and β3-AR agonism alone, and the combination treatment significantly increased the hepatic remnant uptake, albeit the combination did not further increase the hepatic remnant uptake as compared to alirocumab alone (P=0.13) or β3-AR agonism alone (P=0.16). Besides limited power, this may be related to the relatively low dose of alirocumab (1 mg·kg^{-1}·week^{-1}) used in the present study, leading to a modest increase in hepatic LDLR levels (+24%). As a previous study observed higher increases in hepatic LDLR levels (+88% and +133%) at higher doses (3 and 10 mg·kg^{-1}·week^{-1}) in the same mouse model [31], it would be interesting to assess the additive effect of brown fat activation on top of higher doses of alirocumab. It would also be worthwhile to investigate the effects of brown fat activation on top of other PCSK9 inhibitors such as evolocumab. Nevertheless, in our study β3-AR agonism did greatly increase the cholesterol-lowering effect of 1 mg·kg^{-1}·week^{-1} alirocumab to a similar reduction as attained by 3 mg·kg^{-1}·week^{-1} alirocumab in *E3L.CETP* mice [31].

Although it has now been well-established that an increase in HDL-C as induced by genetic variants or CETP inhibitors does not causally reduce cardiovascular disease [32, 33], the cholesterol efflux capacity of HDL is predictive marker for cardiovascular events [34, 35]. Most clinical trials showed that PCSK9 inhibitors only modestly increase HDL-C and ApoA1 levels (i.e. <10%) [36]. Accordingly, we did not observe an effect of alirocumab on HDL-C levels. PCSK9 has been reported to inhibit ATP binding cassette transporter A1-mediated cholesterol efflux induced by liver X receptor and retinoic X receptor agonists [37]. Our study did not show any effect of alirocumab on cholesterol efflux capacity, which could be explained by the low dose of alirocumab used or the difference between both models. In the current study we do show that brown fat activation without and with PCSK9 inhibition increased HDL-C levels as well as the cholesterol efflux capacity of HDL, the key initial step in reverse cholesterol transport. We previously showed that brown fat activation enhances HDL remodeling associated with specific lipidomic changes in both mouse and human HDL [27]. We now add direct evidence that brown fat activation increases surface phospholipid transfer from TRLs to HDL particles, probably promoting HDL remodeling, to enhance the capacity of HDL to induce cholesterol efflux from macrophages. The cholesterol distribution over the lipoproteins indicated that the increased HDL-C is mainly associated with the large HDL fractions (Figure 3A). Previous studies have shown an inverse relationship between HDL size

and CAD risk [38, 39], suggesting that this effect may contribute to the anti-atherogenic effect of brown fat activation.

Inadequate reduction of LDL-C, high levels of TG and low levels of HDL-C are considered to be residual risks to be overcome to further reduce CVD events. Since we observed that brown fat activation enhanced non-HDL-C-lowering effects of anti-PCSK9 treatment, and additively decreased TG and increased HDL-C as well as the cholesterol efflux capacity of HDL on top of anti-PCSK9 treatment, it is tempting to speculate on the relative contribution of these variables to the observed reduction in atherosclerosis development. Linear regression analysis revealed that plasma non-HDL-C exposure markedly correlated with atherosclerotic lesion size (R^2=0.47, P<0.05). Also, TG exposure modestly correlated with lesion size (R^2=0.09, P=0.05), which is likely explained by the fact that plasma TG represents atherogenic TRL remnant levels [40]. In contrast, neither HDL-C exposure (R^2=0.06, P=0.13) nor HDL cholesterol efflux capacity (R^2=0.212; P=0.19) significantly correlated with lesion size. Given the strong correlation between non-HDL-C exposure and lesion size over all experimental groups, brown fat activation on top of PCSK9 inhibition further decreasing non-HDL-C levels may imply further enhanced anti-atherogenic effects. However, the combination therapy did not significantly reduce atherosclerotic lesion area as compared to PCSK9 inhibition alone, which is likely explained by inadequate statistical power and/or the relatively short dietary intervention period. In addition to improving lipid and lipoprotein metabolism, activating brown fat reduces fat mass, improves glucose tolerance and insulin sensitivity [41], and reduces inflammation [42], all of which may also contribute to attenuate atherosclerosis development.

Currently, anti-PCSK9 antibodies belong to the most effective medications to lower cholesterol levels in the clinic. However, despite the recent price cut, approved anti-PCSK9 antibodies including alirocumab and evolocumab are still not as cost-effective as other cholesterol-lowering medications. If the results of the present study can be translated to humans, this may pave a way to increase the cholesterol-lowering effectiveness of anti-PCSK9 treatment by increasing TRL remnant formation via brown fat activation. Human brown fat is metabolically active, even in obese individuals [43] and brown fat activation by means of cold exposure reduces LDL-C levels in hypercholesterolemic patients [44]. Moreover, human white adipose tissue has remarkable plasticity and via browning may contain beige/brite adipocytes with thermogenic properties, which makes them attractive as pharmacological target for the treatment of cardiometabolic diseases [14, 45]. In addition, high brown fat activity is associated with a reduced risk of CVD events [46] and less accumulation of visceral fat [47, 48]. The benefits of brown fat in humans seem further confirmed by a large study examining as many as 139,224 [^{18}F]FDG-PET-CT scans of 53,475 individuals. This study showed that individuals with detectable brown fat have improved glucose, TG and HDL levels, and lower prevalence of cardiometabolic diseases. In addition, these effects of brown fat seem more pronounced in overweight and obesity, indicating that brown fat can overcome the deleterious effects of obesity [49]. Although not monitored in the current study, we previously did not observe any side effects of β3-AR agonism on physical activity [18] and the core body temperature [50] in E3L.CETP mice. Furthermore, a recent study showed that the clinically-approved chronic **β3-AR agonist mirabegron** increases brown fat activity, HDL-C and insulin sensitivity in humans [51]. Although in some FH subjects, due to the mutations of LDLR, the activity of LDLR is impaired, PCSK9 inhibitors still show great cholesterol-lowering effects [9, 10]. This indicates that our combination therapy possibly applies in both normal and FH subjects. Interestingly, a recent study identified that the adipokines leptin and resistin regulate PCSK9 expression, suggesting an additional link between adipose tissue, PCSK9 and

atherosclerosis [52]. Together, these data support the hypothesis that brown fat activation can be combined with PCSK9 inhibition in humans in such a way that dosages of PCSK9 inhibitor can be reduced.

In conclusion, brown fat activation on top of PCSK9 inhibition with alirocumab further improves dyslipidemia by decreasing non-HDL-C via increasing hepatic uptake of cholesterol-enriched TRL remnants and by increasing HDL-C levels and the cholesterol efflux capacity of HDL. Probably by a combination of these mechanisms, combination treatment non-significantly reduces atherosclerotic lesion area compared to PCSK9 inhibition alone and largely reduces atherosclerotic lesion area compared to vehicle. We anticipate that brown fat activation via accelerating lipolytic processing of TRL and increasing TRL remnant formation can further increase the effectiveness of anti-PCSK9 strategy in the treatment of dyslipidemia and CVD in humans.

Acknowledgements

This work was supported by the Netherlands Organisation for Scientific Research-NWO (VENI grant 91617027 to Y.W.); the Netherlands Organisation for Health Research and Development-ZonMW (Early Career Scientist Hotel grant 435004007 to Y.W.); the Netherlands Cardiovascular Research Initiative: an initiative with support of the Dutch Heart Foundation (CVON-GENIUS-2 to P.C.N.R.); and the Netherlands Heart Foundation (2009T038 to P.C.N.R.). Y.W. is supported by the China "Thousand Talents Plan" (Young Talents), Shaanxi province "Thousand Talents Plan" (Young Talents) and Foundation of Xi'an Jiaotong University (Plan A). The authors thank Elsbeth J. Pieterman (TNO-Metabolic Health Research, Gaubius Laboratory, Leiden, The Netherlands) for technical assistance on the fast-performance liquid chromatography. E.Z. is supported by the China Scholarship Council (CSC, grant 201606010321).

Author contributions

E.Z. designed the study, performed experiments, analyzed the data, and drafted the manuscript; Z.L., H.N., and A.C. contributed to animal experiments. S.K. interpreted data and revised the manuscript. J.F.P.B. interpreted data. P.C.N.R. and Y.W. designed the study and revised the manuscript constructively.

Conflict of interest

The authors report no declarations of interest.

References

1. Jukema, J.W., et al., *The controversies of statin therapy: weighing the evidence.* J Am Coll Cardiol, 2012. **60**(10): p. 875-81.
2. Collins, R., et al., *Interpretation of the evidence for the efficacy and safety of statin therapy.* Lancet, 2016. **388**(10059): p. 2532-2561.
3. Cholesterol Treatment Trialists, C., *Efficacy and safety of statin therapy in older people: a meta-analysis of individual participant data from 28 randomised controlled trials.* Lancet, 2019. **393**(10170): p. 407-415.
4. Ruscica, M., et al., *Clinical approach to the inflammatory etiology of cardiovascular diseases.* Pharmacol Res, 2020. **159**: p. 104916.
5. Cohen, J., et al., *Low LDL cholesterol in individuals of African descent resulting from frequent nonsense mutations in PCSK9.* Nat Genet, 2005. **37**(2): p. 161-5.
6. Cohen, J.C., et al., *Sequence variations in PCSK9, low LDL, and protection against coronary heart disease.* N Engl J Med, 2006. **354**(12): p. 1264-72.
7. Koren, M.J., et al., *Anti-PCSK9 monotherapy for hypercholesterolemia: the MENDEL-2 randomized, controlled phase III clinical trial of evolocumab.* J Am Coll Cardiol, 2014. **63**(23): p. 2531-2540.
8. Robinson, J.G., et al., *Efficacy and safety of alirocumab in reducing lipids and cardiovascular events.* N Engl J Med, 2015. **372**(16): p. 1489-99.
9. Kastelein, J.J., et al., *ODYSSEY FH I and FH II: 78 week results with alirocumab treatment in 735 patients with heterozygous familial hypercholesterolaemia.* Eur Heart J, 2015. **36**(43): p. 2996-3003.
10. Raal, F.J., et al., *PCSK9 inhibition with evolocumab (AMG 145) in heterozygous familial hypercholesterolaemia (RUTHERFORD-2): a randomised, double-blind, placebo-controlled trial.* Lancet, 2015. **385**(9965): p. 331-40.
11. Ouellet, V., et al., *Brown adipose tissue oxidative metabolism contributes to energy expenditure during acute cold exposure in humans.* J Clin Invest, 2012. **122**(2): p. 545-52.
12. Labbe, S.M., et al., *In vivo measurement of energy substrate contribution to cold-induced brown adipose tissue thermogenesis.* FASEB J, 2015. **29**(5): p. 2046-58.
13. Giralt, M. and F. Villarroya, *White, brown, beige/brite: different adipose cells for different functions?* Endocrinology, 2013. **154**(9): p. 2992-3000.
14. Sidossis, L. and S. Kajimura, *Brown and beige fat in humans: thermogenic adipocytes that control energy and glucose homeostasis.* J Clin Invest, 2015. **125**(2): p. 478-86.
15. Hoeke, G., et al., *Role of Brown Fat in Lipoprotein Metabolism and Atherosclerosis.* Circ Res, 2016. **118**(1): p. 173-82.
16. Berbee, J.F., et al., *Brown fat activation reduces hypercholesterolaemia and protects from atherosclerosis development.* Nat Commun, 2015. **6**: p. 6356.
17. Zhou, E., et al., *Colesevelam enhances the beneficial effects of brown fat activation on hyperlipidemia and atherosclerosis development.* Cardiovasc Res, 2019.
18. Hoeke, G., et al., *Atorvastatin accelerates clearance of lipoprotein remnants generated by activated brown fat to further reduce hypercholesterolemia and atherosclerosis.* Atherosclerosis, 2017. **267**: p. 116-126.
19. Westerterp, M., et al., *Cholesteryl ester transfer protein decreases high-density lipoprotein and severely aggravates atherosclerosis in APOE*3-Leiden mice.* Arterioscler Thromb Vasc Biol, 2006. **26**(11): p. 2552-9.
20. Landlinger, C., et al., *The AT04A vaccine against proprotein convertase subtilisin/kexin type 9 reduces total cholesterol, vascular inflammation, and atherosclerosis in APOE*3Leiden.CETP mice.* Eur Heart J, 2017. **38**(32): p. 2499-2507.

21. van Vlijmen, B.J., et al., *Modulation of very low density lipoprotein production and clearance contributes to age- and gender- dependent hyperlipoproteinemia in apolipoprotein E3-Leiden transgenic mice.* J Clin Invest, 1996. **97**(5): p. 1184-92.
22. Zadelaar, S., et al., *Mouse models for atherosclerosis and pharmaceutical modifiers.* Arterioscler Thromb Vasc Biol, 2007. **27**(8): p. 1706-21.
23. Zhou, E., et al., *Colesevelam enhances the beneficial effects of brown fat activation on hyperlipidaemia and atherosclerosis development.* Cardiovasc Res, 2020. **116**(10): p. 1710-1720.
24. Rensen, P.C., et al., *Selective liver targeting of antivirals by recombinant chylomicrons--a new therapeutic approach to hepatitis B.* Nat Med, 1995. **1**(3): p. 221-5.
25. Wang, Y., et al., *Prolonged caloric restriction in obese patients with type 2 diabetes mellitus decreases plasma CETP and increases apolipoprotein AI levels without improving the cholesterol efflux properties of HDL.* Diabetes Care, 2011. **34**(12): p. 2576-80.
26. Wong, M.C., et al., *Hepatocyte-specific IKKbeta expression aggravates atherosclerosis development in APOE*3-Leiden mice.* Atherosclerosis, 2012. **220**(2): p. 362-8.
27. Bartelt, A., et al., *Thermogenic adipocytes promote HDL turnover and reverse cholesterol transport.* Nat Commun, 2017. **8**: p. 15010.
28. Blom, D.J., et al., *A 52-week placebo-controlled trial of evolocumab in hyperlipidemia.* N Engl J Med, 2014. **370**(19): p. 1809-19.
29. Khedoe, P.P., et al., *Brown adipose tissue takes up plasma triglycerides mostly after lipolysis.* J Lipid Res, 2015. **56**(1): p. 51-9.
30. Dong, M., et al., *Cold exposure promotes atherosclerotic plaque growth and instability via UCP1-dependent lipolysis.* Cell Metab, 2013. **18**(1): p. 118-29.
31. Kuhnast, S., et al., *Alirocumab inhibits atherosclerosis, improves the plaque morphology, and enhances the effects of a statin.* J Lipid Res, 2014. **55**(10): p. 2103-12.
32. Voight, B.F., et al., *Plasma HDL cholesterol and risk of myocardial infarction: a mendelian randomisation study.* Lancet, 2012. **380**(9841): p. 572-80.
33. Ferri, N., et al., *Present therapeutic role of cholesteryl ester transfer protein inhibitors.* Pharmacol Res, 2018. **128**: p. 29-41.
34. Rohatgi, A., et al., *HDL cholesterol efflux capacity and incident cardiovascular events.* N Engl J Med, 2014. **371**(25): p. 2383-93.
35. Khera, A.V., et al., *Cholesterol efflux capacity, high-density lipoprotein function, and atherosclerosis.* N Engl J Med, 2011. **364**(2): p. 127-35.
36. Filippatos, T.D., et al., *Effects of PCSK9 Inhibitors on Other than Low-Density Lipoprotein Cholesterol Lipid Variables.* J Cardiovasc Pharmacol Ther, 2018. **23**(1): p. 3-12.
37. Adorni, M.P., et al., *Inhibitory effect of PCSK9 on Abca1 protein expression and cholesterol efflux in macrophages.* Atherosclerosis, 2017. **256**: p. 1-6.
38. Mora, S., et al., *Lipoprotein particle profiles by nuclear magnetic resonance compared with standard lipids and apolipoproteins in predicting incident cardiovascular disease in women.* Circulation, 2009. **119**(7): p. 931-9.
39. Mora, S., et al., *Lipoprotein particle size and concentration by nuclear magnetic resonance and incident type 2 diabetes in women.* Diabetes, 2010. **59**(5): p. 1153-60.
40. Nordestgaard, B.G., *Triglyceride-Rich Lipoproteins and Atherosclerotic Cardiovascular Disease: New Insights From Epidemiology, Genetics, and Biology.*

Circ Res, 2016. **118**(4): p. 547-63.
41. Poher, A.L., et al., *Brown adipose tissue activity as a target for the treatment of obesity/insulin resistance.* Front Physiol, 2015. **6**: p. 4.
42. Correa, L.H., G.S. Heyn, and K.G. Magalhaes, *The Impact of the Adipose Organ Plasticity on Inflammation and Cancer Progression.* Cells, 2019. **8**(7).
43. Blondin, D.P., et al., *Selective Impairment of Glucose but Not Fatty Acid or Oxidative Metabolism in Brown Adipose Tissue of Subjects With Type 2 Diabetes.* Diabetes, 2015. **64**(7): p. 2388-97.
44. De Lorenzo, F., et al., *Central cooling effects in patients with hypercholesterolaemia.* Clin Sci (Lond), 1998. **95**(2): p. 213-7.
45. Cereijo, R., M. Giralt, and F. Villarroya, *Thermogenic brown and beige/brite adipogenesis in humans.* Ann Med, 2015. **47**(2): p. 169-77.
46. Takx, R.A., et al., *Supraclavicular Brown Adipose Tissue 18F-FDG Uptake and Cardiovascular Disease.* J Nucl Med, 2016. **57**(8): p. 1221-5.
47. Brendle, C., et al., *Correlation of Brown Adipose Tissue with Other Body Fat Compartments and Patient Characteristics: A Retrospective Analysis in a Large Patient Cohort Using PET/CT.* Acad Radiol, 2018. **25**(1): p. 102-110.
48. Wang, Q., et al., *Brown adipose tissue activation is inversely related to central obesity and metabolic parameters in adult human.* PLoS One, 2015. **10**(4): p. e0123795.
49. Becher, T., et al., *Brown adipose tissue is associated with cardiometabolic health.* Nat Med, 2021. **27**(1): p. 58-65.
50. Li, Z., et al., *Electrical Neurostimulation Promotes Brown Adipose Tissue Thermogenesis.* Front Endocrinol (Lausanne), 2020. **11**: p. 567545.
51. O'Mara, A.E., et al., *Chronic mirabegron treatment increases human brown fat, HDL cholesterol, and insulin sensitivity.* J Clin Invest, 2020. **130**(5): p. 2209-2219.
52. Macchi, C., et al., *Leptin, Resistin, and Proprotein Convertase Subtilisin/Kexin Type 9: The Role of STAT3.* Am J Pathol, 2020. **190**(11): p. 2226-2236.

Supplemental appendix

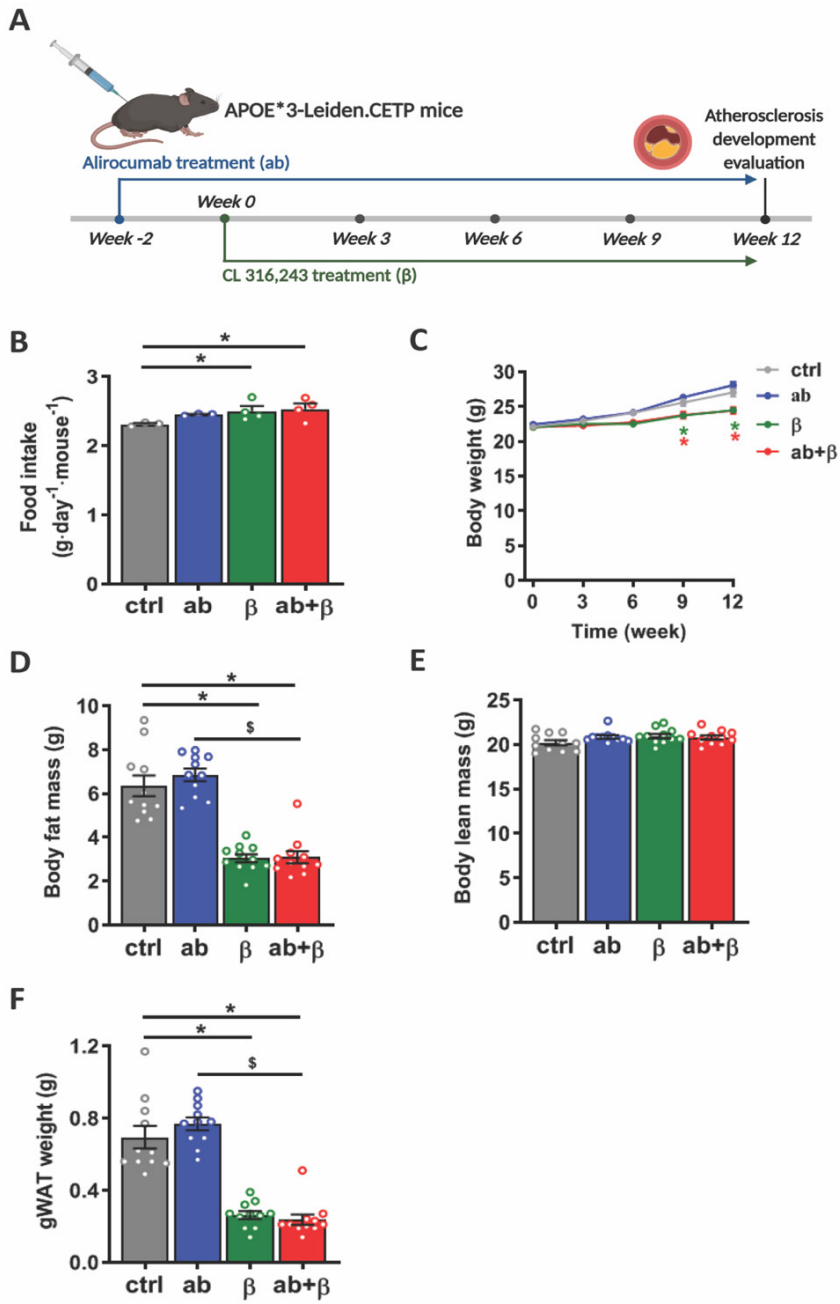

Supplemental Figure 1. β3-AR agonism on top of anti-PCSK9 treatment decreases body fat mass and gonadal white adipose tissue. *E3L.CETP* mice fed a WTD and pretreated with vehicle (ctrl) or the anti-PCSK9 antibody alirocumab (ab) from week -2, were cotreated with vehicle or the β3-AR agonist CL316,243 (β) from week 0 for additional 12 weeks. (**A**) The experimental setup is shown. (**B**) Food intake was determined during the first three weeks of the treatment. Mice were group housed (11 mice per group). Individual values represent

the average food intake of each cage (n= 3, 3, 4 and 4 cages, respectively). (**C**) Body weight was measured every three weeks. After 12 weeks, (**D**) body fat mass and (**E**) lean mass were evaluated. (**F**) Mice were killed and gonadal white adipose tissue (gWAT) was isolated and weighed (n = 11 mice per group). Values are means ± SEM. Differences between 4 groups were determined using one-way ANOVA with the *LSD post hoc* test. *P<0.05 vs. vehicle (ctrl); $P<0.05 vs. anti-PCSK9 antibody (ab).

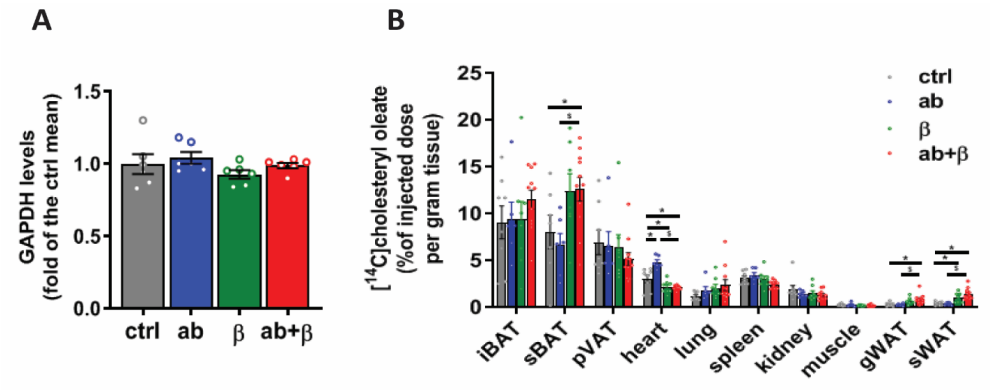

Supplemental Figure 2. Effects of β3-AR agonism on top of anti-PCSK9 treatment on organ uptake of [^{14}C]**cholesteryl oleate-labelled TRL-like particles.** *E3L.CETP* mice fed a WTD and pretreated with vehicle (ctrl) or the anti-PCSK9 antibody alirocumab (ab) from week -2, were cotreated with vehicle or the β3-AR agonist CL316,243 (β) from week 0. At week 3, mice were injected with [^{14}C]cholesteryl oleate (CO)-labelled TRL-like particles. After 15 min mice were killed. (**A**) Livers were collected to evaluate GAPDH protein levels (6 out of 11 mice were randomly tested in each group), and (**B**) various organs were collected and weighed to determine uptake of [^{14}C]CO. gonadal while adipose tissue, gWAT; interscapular brown fat, iBAT; perivascular adipose tissue, pVAT; subscapular brown fat, sBAT; subcutaneous white adipose tissue, sWAT (n = 8, 6, 8, 11 mice per group, respectively). Mice were excluded in case of technical failure of injection. Values are means ± SEM. Differences between 4 groups were determined using one-way ANOVA with the *LSD post hoc* test. *P<0.05 vs. vehicle (ctrl); $P<0.05 vs. anti-PCSK9 antibody (ab).

2

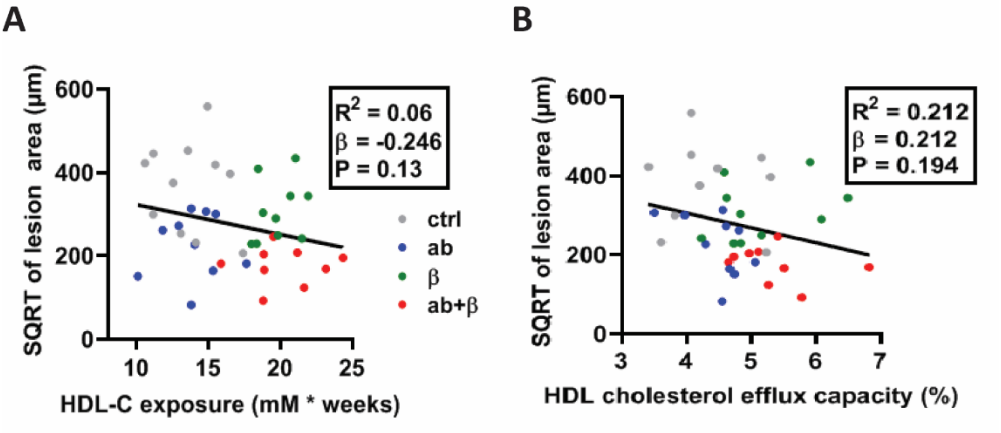

Supplemental Figure 3. HDL-cholesterol level and cholesterol efflux capacity of HDL do not correlate with atherosclerotic lesion area. *E3L.CETP* mice fed a WTD and pretreated with vehicle (ctrl) or the anti-PCSK9 antibody Alirocumab (ab) from week -2, were cotreated with vehicle or the β3-AR agonist CL316,243 (β) from week 0 for 12 additional weeks. Cross-sections of aortic root were stained with hematoxylin-phloxine-saffron to determine atherosclerotic lesion area. The square root (SQRT) of the mean atherosclerotic lesion area was plotted against the plasma (**A**) HDL-cholesterol (-C) exposure and (**B**) cholesterol efflux capacity to HDL (n = 11, 10, 10 and 10 mice, respectively). Three samples were lost due to technical failure of staining.